Improved photocatalytic H_2 production from aqueous glucose biomass by oxidized g-C_3N_4

Andrea Speltini*, Andrea Scalabrini, Federica Maraschi, Michela Sturini, Ambra Pisanu, Lorenzo Malavasi, Antonella Profumo

Department of Chemistry, University of Pavia, via Taramelli 12, 27100 Pavia (Italy)

**E-mail: andrea.speltini@unipv.it (A. Speltini)*

Fax: +39 0382-528544; Tel.: +39 0382-987349

Abstract

Chemically modified g-C_3N_4 for the photocatalytic H_2 evolution from water was explored. Bulk g-C_3N_4 was treated in hot HNO_3 aqueous solution to obtain the oxidized material (o-g-C_3N_4), tested in water containing glucose as model sacrificial biomass, using Pt as co-catalyst, under simulated solar light. The behaviour of o-g-C_3N_4 was studied in relation with catalyst amount, Pt loading, glucose concentration. Results showed that H_2 production is favoured by increasing glucose concentration up to 0.1 M and Pt loading up to 3 wt%, and it resulted strongly enhanced using small amount of o-g-C_3N_4 (0.25 g L^{-1}). o-g-C_3N_4 possesses superior photocatalytic activity (~ 26-fold higher) compared to pristine g-C_3N_4, with H_2 evolution further improved by ultrasound-assisted exfoliation and yields up to ca. 1370 μmoles h^{-1} per gram of catalyst, with excellent reproducibility (RSD < 6 %, *n*=3). Significant production was observed also in river and sea waters, with results far better (up to ca. 2500 μmoles g^{-1} h^{-1}) compared to commercial P25 TiO_2 under natural solar light.

Keywords

biomass; graphitic carbon nitride; hydrogen; photocatalysis; solar light

1. Introduction

Nowadays, the increasing global crisis of energy shortage and environmental issues are becoming serious threats to the long-term development of human society. Among the potential solutions, photocatalysis is emerging with tremendous potentiality as it is a low-cost, renewable, clean, and safe technology that just requires solar light as a driving force, and a suitable semiconductor as a photocatalyst to carry out reactions for a variety of applications, including hydrogen gas (H_2) production from water [1].

H_2 is an appealing storable energy source because of its efficient conversion in fuel cells with water as the only by-product. To date, the largest part of the produced H_2 derives from natural gas through steam-methane reforming, and only about 5 % is obtained from renewable resources, mostly *via* water electrolysis. Nevertheless, H_2 production based on natural gas involves some dilemmas because of the limited availability of fossil fuels and the consistent amounts of carbon dioxide released in the atmosphere. With regard to H_2 evolution from water, several photocatalytic systems have been improved by addition of organic additives as the sacrificial agents that, undergoing oxidation, are able to enhance water reduction to give gas-phase H_2 [2,3]. Various inorganic catalysts have been studied under UV or visible light, including ZnO, CdS, TiO_2, SnO_2, $BiVO_4$, Cu_2O, Fe_2O_3. However, the serious drawback common to all these materials is the low photocatalytic efficiency, caused by the fast charge carriers recombination. This can be slowed down by immobilization of co-catalysts (e.g. noble metals) onto the surface of the photocatalysts, which not only improves the charge separation by capturing electrons or holes, but also favours the surface catalytic reaction by reducing the activation energy [4].

Among the inorganic semiconductors, TiO_2 is the most used because of its chemical stability, low cost and non-toxicity. Regardless of the advances achieved by TiO_2-based photocatalysis for environmental purification and solar energy conversion [5,6], the practical application of TiO_2 is drastically limited because of the partial absorption of natural sunlight. In fact, TiO_2 absorbs mainly the UV component of solar light (< 387 nm), that represents only 4-5 % of the solar spectrum [2].

For this reason, it is of overwhelming importance to shift light absorption toward the visible region, and different approaches, including modification of TiO_2 by element doping, dye-sensitization and coupling with heterogeneous semiconductors, as well as development of new non-TiO_2 based photocatalytic systems, have been employed to harvest much more visible light, thus enhancing the photocatalytic performance [4].

In the framework of novel advanced materials, graphitic carbon nitride (g-C_3N_4) has caught plenty of interest in the recent years for a number of applications, including (photo)electrochemical energy conversion [1,7] and analytical determinations [8-10] because of its unique properties. This material is a metal-free polymer semiconductor, with a graphitic-like layered structure consisting of 2D sheets composed of tris-s-triazines interconnected *via* tertiary amines. It can be easily synthesized from a variety of low-cost nitrogen-containing compounds (e.g. dicyandiamide, melamine, urea, etc.) by thermal condensation, obtaining different physical-chemical properties as function of the reaction conditions [11,12].

Since being introduced in the field of heterogeneous catalysis in 2006 [13], g-C_3N_4 has been largely studied as visible-light-driven catalyst for CO_2 reduction [14], organic syntheses [15], abatement of pollutants [16], and H_2 production from water [4,11,17], documented for the first time in 2009 [18]. In the field of photocatalysis, its great potentiality mainly relies on its band gap (~ 2.7 eV) smaller compared to TiO_2. The possibility to be exfoliated into 2D thin nanosheets endows with high aspect-ratio, large surface area and high-density of functional groups for anchoring co-catalysts which greatly improve the overall photocatalytic performance [4,17,19].

With regard to H_2 photoproduction, in order to compensate for the high recombination of photo-excited charge carriers and to further narrow the band gap, g-C_3N_4 has been tested after modification with conductive carbon materials, nanodiamonds, metal co-catalysts and other semiconductors, or by heteroatoms doping [11,17,18,20]. The more negative conduction band of g-C_3N_4 compared to TiO_2 indicates a much stronger reduction capability of photo-induced electrons that, joined with visible light absorption and proper physical-chemical modification of the bulk

78 material, could lead to tremendous H_2 production improvements [4,17,21]. Recent works showed
79 that the photocatalytic activity of bulk g-C_3N_4 can be enlarged by thermal oxidation (in air or
80 oxygen atmosphere), due to a synergistic effect of enlarged surface area, enhanced reduction
81 capability, improved electron transport ability and prolonged lifetime of charge carriers [17,19]. A
82 remarkable improvement in the photocatalytic efficiency of bulk g-C_3N_4 has been achieved by
83 thermal oxidation followed by a solvothermal treatment involving use of polyvinylpyrrolidone and
84 hexadecyl trimethyl ammonium bromide [22]. As a matter of fact, in presence of Pt as co-catalyst
85 and triethanolamine (TEOA) as sacrificial agent, H_2 yields up to ca. 1500 μmoles g^{-1} h^{-1} were
86 achieved under visible light [17,19,22]. Under simulated solar light, production up to ca. 2800
87 μmoles g^{-1} h^{-1} was reached from aqueous methanol by post-synthesis derivatization of bulk g-C_3N_4
88 with urea groups, using Pt co-catalyst [23]. Therefore, oxidation of g-C_3N_4 appears to be an
89 interesting route to improve its catalytic performance. However, most of the oxidation processes
90 used nowadays require relatively complex methods and/or post-oxidation processing and cannot be
91 considered as a viable route to scale-up the production of oxidized g-C_3N_4. In order to achieve a
92 very active material by oxidation, while keeping at minimum the synthetic efforts, the present
93 authors explored the photocatalytic performance of g-C_3N_4 oxidized by nitric acid refluxing. In
94 addition, to the authors' best knowledge, neither bulk g-C_3N_4 nor (chemically)modified g-C_3N_4 have
95 been to date investigated for the photocatalytic H_2 production from water in presence of biomass
96 sacrificial agents, which are more cost-effective and eco-friendly than fine chemicals such as TEOA
97 and methanol used as the electrondonor substrates. Finally, the chemically modified g-C_3N_4
98 materials recently described in the literature have not been tested under sunlight outdoor conditions.
99 On the basis of the current state of the art, in this work bulk g-C_3N_4 prepared by thermal
100 condensation of dicyandiamide (DCD) was treated in HNO_3 aqueous solution, and characterized by
101 various techniques, i.e. X-ray powder diffraction (XRD), scanning electron microscopy (SEM),
102 diffuse reflectance UV-Vis spectroscopy (DRS), Brunauer, Emmett and Teller (BET) surface area
103 and point of zero charge (pH_{PZC}) measurements. The obtained material (o-g-C_3N_4) was studied as

104 the catalyst for the H_2 photoproduction from glucose aqueous solution, under simulated solar light,
105 using Pt as the co-catalyst. The factors involved in the photocatalytic process have been
106 investigated, that is g-C_3N_4 concentration, Pt amount, sacrificial agent concentration, solution pH,
107 and effect of ultrasound exfoliation. H_2 photoproduction was also investigated in environmental
108 waters, under natural sunlight (outdoor conditions). In addition, comparative experiments were
109 performed using the well-known, commercial P25 TiO_2 catalyst.
110
111 **2. Experimental section**
112 *2.1. Chemicals and materials*
113 H_2PtCl_6 (~ 38 % Pt basis), DCD (99 %), HNO_3 (65 %, w/w), TEOA (≥ 99 %) and 0.45 μm nylon
114 filters were supplied by Sigma-Aldrich (Milan, Italy). Glucose (> 99 %, w/w), NaOH (97 %, w/w)
115 and H_2SO_4 (96 %, w/w) were purchased from Carlo Erba Reagents (Milan, Italy). Ar (99.999 %),
116 N_2 (99.999 %) and H_2 (99.995 %) high purity standard gases were supplied by Sapio S.r.l. (Milan,
117 Italy). Evonik P25 TiO_2 (80 % anatase, 20 % rutile, particle size 30 nm, surface area 50 ± 15 m^2 g^{-1})
118 was purchased from Evonik Industries AG (Hanau, Germany).
119
120 *2.2. Synthesis and characterization of the photocatalysts*
121 g-C_3N_4 was synthesized from the polymerization of DCD with the following thermal treatment
122 (under N_2 flow): heating (10 °C min^{-1}) to 500 °C, isothermal step for 4 h followed by cooling to
123 room temperature (1 °C min^{-1}). Yield of this reaction is around 60 %.
124 The chemically-modified catalyst (o-g-C_3N_4) was prepared by refluxing 1 g of g-C_3N_4 in 100 mL
125 aqueous HNO_3 (1:1 dilution, 7.3 M) for 3 h [24], under magnetic stirring. The suspension was then
126 filtered and the whitish solid collected was washed with plenty of distilled water until neutrality of
127 the eluate, and dried in oven (60 °C, 24 h). The yield of the oxidation step was 52 %, with an
128 excellent batch-to-batch reproducibility experimentally verified (RSD < 9 %, n=4). Before use, o-g-
129 C_3N_4 was manually homogenized in a mortar.

130 The pH_{PZC} was determined by the immersion technique [25]. For each catalyst, 30 mg were
131 suspended in 2.5 mL 0.03 M KNO_3 solutions adjusted at different pH values (in the range 2-12),
132 and the suspension was shaken for 24 h at 250 rpm until equilibrium pH was reached. The pH
133 variation (ΔpH) during equilibration was wrote down and the pH_{PZC} was identified as the initial pH
134 providing the minimum ΔpH.
135 The crystal structure of the samples has been characterized by room temperature Cu-radiation XRD
136 acquired with a Bruker D8 diffractometer.
137 Microstructural characterization of the samples was made using a high-resolution scanning electron
138 microscope (SEM, TESCAN Mira 3) operated at 25 kV.
139 Surface area measures were carried out according to BET single point method by means of a
140 Flowsorb II 2300 (Micromeritics, US) apparatus. Each sample was accurately weighed (about 0.8 g)
141 and degassed at 80 °C for 1.5 h under a continuous stream of a N_2:He 30:70 mixture. Gas
142 adsorption was then achieved by placing the sample in liquid nitrogen. Three replicates were done
143 for each sample.
144 DRS spectra were acquired in the wavelength range 300-800 nm directly on the powders by using a
145 Jasco V-750 spectrophotometer, equipped with an integrating sphere (Jasco ISV-922). Quartz
146 cuvettes with 1 mm optical path were used.
147
148 *2.3. Sample preparation and photocatalytic tests*
149 Experiments were conducted on glucose aqueous solutions (0.01-1 M in distilled water) irradiated
150 in Pyrex glass containers (28 mL capacity, 21 mL sample [26]). After addition of the catalyst (0.25-
151 2 g L^{-1}), the sample (sonicated for 20 min or not) was deoxygenated by Ar bubbling (20 min) to
152 obtain anoxic conditions, and irradiated under magnetic stirring for 6 h. Pt was loaded on the
153 catalyst surface (0.1-3 wt%) by *in situ* photodeposition using H_2PtCl_6 [17,19]. Solution pH was
154 investigated in the range 2-11 by addition of aqueous NaOH or H_2SO_4. Irradiation was performed
155 under simulated solar light using a Solar Box 1500e (CO.FO.ME.GRA S.r.l., Milan, Italy) set at a

power factor 500 W m^{-2}, and equipped with UV outdoor filter of soda lime glass IR treated. The photon flux was determined experimentally by 2-nitrobenzaldehyde actinometry [27].

Environmental waters, tested instead of distilled water, were collected from Ticino River (Pavia, Italy) and from the Ligurian sea (Northern Italy); physical-chemical parameters are reported in Table S1 (Supplementary Material). Irradiation tests under natural solar light were performed in Pavia over three non-consecutive days (45°11'46'' N, 9°09'38'' E, mid June 2017, 10.00 a.m.–4.00 p.m., 27–33 °C, relative humidity 25-47 %). The mean global radiation was 797 W m^{-2} (see Supplementary Material Fig. S1).

Triplicate experiments were always performed. The headspace evolved gas was quantified by gas chromatography coupled with thermal conductivity detection (GC-TCD), as described in previous work (injection volumes 0.1-2 mL) [28]. All the results are expressed in terms of H_2 evolution rate, as μmoles of gas per gram of catalyst per hour (μmoles g^{-1} h^{-1}).

3. Results and discussion

3.1. Characterization of the photocatalysts

Fig. 1 presents the XRD diffraction patterns of the as-prepared g-C_3N_4 and of the g-C_3N_4 sample oxidized for 3 h. The XRD pattern of the as-prepared sample ("as-prep" in Fig. 1) is in agreement with literature [18], showing a first peak around 12.5°, attributed to the (100) plane, due to the intralayer *d*-spacing, and a main peak at 2θ ca. 27°, reported as the (002) plane, ascribed to the distance between the layers of the graphitic material. By performing a 3 h oxidation the pattern (3 h in Fig. 1) shows a reduction of the intensity of the (100) reflection due to a possible disorder introduced in the carbon nitride planes by the oxidation process. In addition, the main peak shifts at higher angle, i.e. from 27.5044(7)° to 27.5707(7)° passing from the as-prepared sample to the one oxidized for 3 h, indicating a contraction of the interlayer distance. Such effect has been correlated to the increased interaction induced by the more electronegative O-atoms replacing the C-atoms in the layers [17], and it turns in accordance with the reduction of the pH_{PZC} (see later in the text).

Selected SEM images at 100 kx magnification for the as-prepared and 3 h oxidized samples are reported in Figs. 2a and 2b, respectively. As it can be seen, the samples are made by grains of irregular shape with sizes from the hundreds of nm to microns range with the typical stacked lamellar structure and plate-like morphology of g-C_3N_4. From the images it is clear an increase of surface roughness for the sample treated under nitric acid with respect to the untreated g-C_3N_4.

This result is in accordance with the surface area enhancement observed after oxidation. Indeed, BET measurements indicate an increase of the surface area passing from the as-prepared sample (6.1 $m^2\ g^{-1}$) to the oxidized sample (12.3 $m^2\ g^{-1}$). The pH_{PZC} varied from 6 to 5.2 for the pristine and the oxidized materials, respectively, further supporting the formation of oxygenated ionisable functionalities on the modified catalyst. The inclusion of oxygen-rich groups has been verified by XPS, where a total increase of the O-content has been observed from the O1s signal, together with an increase of C=O groups assessed from C1s (discussed in ref. [24]).

Diffuse reflectance measurements show a slight blue-shift passing from the as-prepared to the oxidized sample (see Fig. S2, Supplementary Material). Accordingly, the band-gap determined by the reflectance are 2.70 and 2.77 eV for g-C_3N_4 and the oxidized material, respectively (the pale yellow material turns to a whitish colour after HNO_3 treatment).

3.2. H_2 photoproduction experiments

The as prepared bulk catalyst and the same material submitted to oxidation (o-g-C_3N_4) were tested in parallel for the H_2 photoproduction from water. Preliminary tests were performed under simulated solar light using 1 M glucose aqueous solutions, with no pH modification, in presence of 0.25 g L^{-1} catalyst and 3 wt% Pt immobilized on the catalyst by *in situ* photodeposition.

As shown in Table 1, results indicated a 26-fold higher H_2 evolution activity for the o-g-C_3N_4 compared to the g-C_3N_4 semiconductor. Under the same conditions, a great H_2 production improvement was obtained by 20 min sonication of the catalyst suspension before irradiation, with

207 H_2 evolution far larger (17-folds) in presence of o-g-C_3N_4 compared to g-C_3N_4, due to and
208 exfoliation effect that is in agreement with previous work [16].
209 As it is highlighted in Table 2, these enhancements are outstanding to those achieved by the newly
210 proposed co-condensed amorphous carbon/g-C_3N_4 composite [29] that showed a 10-fold increased
211 H_2 production towards pure g-C_3N_4, with maximum rates of ca. 213 μmoles g^{-1} h^{-1}. Moreover, o-g-
212 C_3N_4 is attractive compared to the g-C_3N_4 modified by thermal exfoliation followed by
213 solvothermal treatment [22], and also to coupling with mesoporous carbon [30] or urea-
214 modification by a two-step post-synthesis derivatization [23]. These considerations are further
215 strengthened by considering that the present modification process of g-C_3N_4 is very simple and
216 cost-effective with respect to most of the modifications actually proposed in the current literature.
217 The enhancement of the photocatalytic activity here gained is also far higher than that reached by
218 one-pot O_2-thermal oxidation [17] and gaseous stripping in wet N_2 [31].
219 These considerations are also well corroborated by a further test carried out in aqueous TEOA (10
220 %, v/v), using 1 g L^{-1} o-g-C_3N_4 (3 wt% Pt), that provided a H_2 evolution rate higher than 3000
221 μmoles g^{-1} h^{-1} (Table 2). The inter-day precision of the above experiments, evaluated on three non-
222 consecutive days on independent samples prepared and irradiated under the above conditions,
223 showed relative standard deviations (RSDs) not higher than 6 %.
224 To explain the better performance of o-g-C_3N_4 compared to the as-prepared semiconductor we can
225 consider both the physical-chemical and the electronic properties of the semiconductor, viz. surface
226 area, band gap and pH_{PZC}, recognized to be key properties accounting for the overall photocatalytic
227 activity [32]. Since there is no significant difference in terms of absorption spectra before and after
228 oxidation (band gap 2.70 eV vs. 2.77 eV, respectively), the superior behaviour of o-g-C_3N_4 in terms
229 of H_2 production can be attributed in first instance to the higher surface area, resulting in more
230 active sites available for the photoreaction [17,32]. Another fundamental reason relies in the
231 chemical modification. Indeed, insertion of oxygen-containing functional groups by chemical
232 oxidation greatly favours the material dispersion in aqueous solution and further enhances its

interfacial coupling and photocatalytic activity [32]. Moreover, it is reasonable to assume that the oxygenated groups in the carbon nitride framework decrease the electron-hole recombination rate and generate an electron-rich state in the semiconductor, with a consequent higher reduction ability, similarly to thermally oxidized g-C_3N_4 [17].

In view of the above reported data, o-g-C_3N_4 was selected for further investigations, as described below. Firstly, the role of the catalyst was confirmed by control tests carried out omitting either o-g-C_3N_4 or Pt and observing undetectable H_2 evolution ($< 3 \times 10^{-3}$ μmoles, ≡ IDL); on the other hand, no H_2 was detected in darkness, as expected. The contribution of direct water splitting was evaluated by irradiation of pure water samples (with no glucose), and it was found to be negligible (2 μmoles g^{-1} h^{-1}), thus highlighting the key role of the sacrificial biomass in sustaining the photocatalytic H_2 evolution from water. These tests give evidence of a photoreaction mechanism typical of photocatalytic systems for H_2 evolution from water, with Pt co-catalyst as the water hydrogen ion reduction site and glucose as the sacrificial valence band holes scavenger, as reported for g-C_3N_4 systems [29,31,32].

Prompted by such findings, we investigated the effects of the main operational parameters involved in the photocatalytic system, i.e. glucose concentration, catalyst amount, co-catalyst loading, and sample pH [2,26,33-35].

As shown in Fig. 3a, the sacrificial donor concentration affected the photoreaction, with improved H_2 yields in going from 0.01 to 0.1 M. The profile shows a quasi-linear increase of the production rate in the concentration range 0.01-0.04 M, with a plateau maintained for more concentrated solutions. This can be described as a Langmuirian catalytic behaviour, reported in literature for the H_2 photocatalytic production from aqueous glucose [34,35], and it indicates that the reaction depends on the glucose amount present on the catalyst surface rather than in the solution. In particular, at a low sacrificial biomass concentration, the rate of the photocatalytic reaction is limited by the mass transfer of glucose from the bulk to the o-g-C_3N_4 surface, while in more

concentrated solutions the interfacial reactions dominate the process, as a consequence of the gradual adsorption and saturation of glucose on the catalyst surface [34].

The correlation between the H_2 yields and the amount of co-catalyst, explored in the range 0.1-3 wt%, is shown in Fig. 3b; according to previous work [18] higher Pt loadings were not considered, to avoid both shielding of incident light and decrease of the catalyst reactive surface [2]. The highest efficiency was observed with 3 wt% Pt, that is indeed the amount usually reported in the literature for (modified) g-C_3N_4 catalysts [11,17,18,36].

The study of the catalyst amount effect gave interesting results: by increasing the o-g-C_3N_4 concentration up to 2 g L^{-1}, the amount of evolved gas was strongly lowered (Fig. 4a), indicating that small amounts of o-g-C_3N_4 are able to efficiently catalyse glucose oxidation, hence enhancing H_2 production from water. The trend can be explained by the excessive light scattering that occurs using increasing amounts of ultrasound-exfoliated o-g-C_3N_4, according to the 2D graphitic structure of this semiconductor. This behaviour is also supported by the trend usually observed for a well-known, *non-exfoliable* material as P25 TiO_2 that provides an increase of the H_2 production as a function of the catalyst concentration [26,28,33,37], only in the optimal concentration range (0.5-3 g L^{-1}) [38].

Being the pH the key parameter in controlling the adsorption equilibrium of the substrate on the catalyst surface in heterogeneous photocatalytic systems [33,34], the effect of solution pH was investigated. It was observed that altering the solution pH an increase of H_2 evolution was noticed, both under acidic or alkaline conditions (Fig. 4b), with the highest production rate achieved at pH 11 (ca. 1370 μmoles g^{-1} h^{-1}). The effect of solution pH on the H_2 evolution is very intricate, involving the changes of the surface charge of catalyst and the chemical state of glucose (undissociated in the pH range investigated, (pK_a ca. 12.3) [34]. The different H_2 yields obtained could be explained by a combination of different factors. Among these, the variation of the molecular glucose affinity for the negatively or positively charged o-g-C_3N_4 surface (pH_{PZC} 5.2, experimentally determined, see Section 2.2) and, consequently, the positions of the catalyst

284 conduction and valence bands with respect to those of the redox couples in solution [39], thus
285 glucose scavenger ability toward the o-g-C_3N_4 valence band holes. Other possible explanations can
286 be found considering the better dispersibility and the higher hydrophilicity of the catalyst, charged
287 in aqueous solution above and below the pH_{PZC} [32].
288 With the aim to improve the sustainability of the process, the photoproduction was investigated also
289 in actual environmental waters. Irradiation tests performed in not tampered river and seawater
290 samples (native pH) by using the optimized parameters defined above for distilled water (i.e. 0.1 M
291 glucose, 0.25 g L^{-1} o-g-C_3N_4, 3 wt% Pt), led to H_2 evolution rates totally comparable to those in
292 distilled water (see Table 3). This key result substantially demonstrates for the first time the use of
293 o-g-C_3N_4 as an efficient catalyst for green H_2 production.
294 The system was characterized in terms of turnover number (TON) and apparent quantum yield
295 (AQY), both calculated on the results observed in distilled water. The TON, calculated as the ratio
296 H_2 moles/Pt moles, ranged from 33 (at native pH) to 53 (at pH 11), thus indicating that Pt
297 effectively catalyses hydrogen ions reduction to give gas phase hydrogen. The AQY, calculated as
298 H_2 moles/moles of incident photons (flux 1.53×10^{-7} moles photons s^{-1}, determined according to
299 ref. [27]), was 0.8 % (at native pH) and 1.3 % under alkaline conditions (pH 11).
300 As shown in Table 3, the system was able to efficiently work also under sunlight (outdoor
301 conditions), reaching productions up to ca. 2500 μmoles g^{-1} h^{-1}. This value, higher compared to the
302 mean production observed by solar simulated light, can be explained considering the global
303 radiation registered under outdoor conditions (mid June), higher than the one selected for the solar
304 box experiments (see Section 2.3 and Supplementary Material, Fig. S1).
305 The behaviour of o-g-C_3N_4 was compared in parallel to that of the well-known P25 TiO_2 under
306 sunlight (6 h). Experiments were conducted in seawater (native pH) under the most convenient
307 conditions used in aqueous glucose for each catalyst (for TiO_2 according to literature [34]) and, in
308 addition, TiO_2 was also tested under the same conditions selected for o-g-C_3N_4 according to the
309 previous discussion (0.1 M glucose, 3 wt% Pt, 0.25 g L^{-1} catalyst). With hydrogen productions of

577 and 485 μmoles g^{-1} h^{-1} respectively, and in spite of its far higher surface area (50 m^2 g^{-1}), it was found that the commercial semiconductor provides a lower H_2 evolution activity compared to the o-g-C_3N_4 presented in this work (ca. 2500 μmoles g^{-1} h^{-1}, see Table 3). The superior results achieved under sunlight usingo-g-C_3N_4 compared to P25 TiO_2 are certainly due to the combination of the peculiar properties of the g-C_3N_4, that is higher visible-light harvesting and stronger reduction ability [4], with the improved photocatalytic activity achieved after its oxidation. Such findings unquestionably support the great potential of o-g-C_3N_4 for sunlight-driven photocatalysis.

4. Conclusions

A novel application of chemically modified g-C_3N_4 for the photocatalytic H_2 evolution from water, in presence of glucose biomass as the sacrificial agent is described. The bulk material, easily prepared by thermal condensation of dicyandiamide, was characterized before and after the one-pot oxidation in HNO_3. The modified material (o-g-C_3N_4) showed a significantly higher H_2 evolution activity under simulated solar light compared to the pristine material, further enhanced by sonication before irradiation. The system is also able to produce H_2 under natural sunlight and from raw environmental waters, with results comparable to those obtained in distilled water. A superior H_2 production of o-g-C_3N_4 compared to P25 TiO_2 under natural solar light is clearly shown. Overall, the results presented here suggest the real use of modified g-C_3N_4 for H_2 evolution using sacrificial biomass, and its possible further extension to other photocatalytic applications.

Acknowledgments

Dr. Ilenia Tredici is acknowledged for the scientific support in the SEM analysis performed at the CISRiC (Centro Interdipartimentale di Studi e Ricerche per la Conservazione del Patrimonio Culturale) of Pavia. This work was partially supported by CATSTER Project within the framework of the Lombardy Region-INSTM Agreement (2015).

336 **References**

337 [1] Cao S, Low J, Yu J, Jaroniec M. Polymeric photocatalysts based on graphitic carbon nitride.
338 Adv Mater 2015;27:2150-76.

339

340 [2] Leung DYC, Fu X, Wang C, Ni M, Leung MKH, Wang X, Fu X. Hydrogen production over
341 titania-based photocatalysts. Chem Sus Chem 2010;3:681-94.

342

343 [3] Bowker M. Photocatalytic hydrogen production and oxygenate photoreforming. Catal Lett
344 2012;142:923-9.

345

346 [4] Dong X, Cheng F. Recent developments in exfoliated two-dimensional g-C_3N_4 nanosheets for
347 photocatalytic applications. J Mater Chem 2015;3:23642-52.

348

349 [5] Matsuoka M, Anpo M. Applications of environmentally friendly TiO_2 photocatalysts in green
350 chemistry: environmental purification and clean energy production under solar light irradiation. In:
351 Handbook of Green Chemistry, Weinheim: Wiley-VCH; 2010, p. 59-80.

352

353 [6] Sturini M, Rivagli E, Maraschi F, Speltini A, Profumo A, Albini A. Photocatalytic reduction of
354 vanadium(V) in TiO_2 suspension: chemometric optimization and application to wastewaters. J
355 Hazard Mater 2013;254-255:179-84.

356

357 [7] Liu J, Wang H, Antonietti M. Graphitic carbon nitride ‘‘reloaded’’: emerging applications
358 beyond (photo)catalysis. Chem Soc Rev 2016;45:2308-26.

359

[8] Sun YP, Ha W, Chen J, Qi HY, Shi YP. Advances and applications of graphitic carbon nitride as sorbent in analytical chemistry for sample pretreatment: a review. Trend Anal Chem 2016;84:12-21.

[9] Speltini A, Sturini M, Maraschi F, Profumo A. Recent trends in the application of the newest carbonaceous materials for magnetic solid-phase extraction of environmental pollutants. Trend Environ Anal Chem 206;10:11-23.

[10] Speltini A, Maraschi F, Govoni R, Milanese C, Profumo A, Malavasi L, Sturini M. Facile and fast preparation of low-cost silica-supported graphitic carbon nitride for solid-phase extraction of fluoroquinolone drugs from environmental waters. J Chromatogr A 2017;1489:9-17.

[11] Martin DJ, Qiu K, Shevlin SA, Handoko AD, Chen X, Guo Z, Tang J. Highly efficient photocatalytic H_2 evolution from water using visible light and structure-controlled graphitic carbon nitride. Angew Chem Int Ed 2014;53:9240-5.

[12] Lin L, Ou H, Zhang Y, Wang X. Tri-s-triazine-based crystalline graphitic carbon nitrides for highly efficient hydrogen evolution photocatalysis. ACS Catal 2016;6:3921-31.

[13] Goettmann F, Fischer A, Antonietti M, Thomas A. Chemical synthesis of mesoporous carbon nitrides using hard templates and their use as a metal-free catalyst for Friedel-Crafts reaction of benzene. Angew Chem Int Ed 2006;45:4467-71.

[14] Shi L, Wang T, Zhang H, Chang K, Ye J. Electrostatic self-assembly of nanosized carbon nitride nanosheet onto a zirconium metal–organic framework for enhanced photocatalytic CO_2 reduction. Adv Funct Mater 2015;25:5360-7.

[15] Lin X, Zhao S, Chen Y, Fu L, Zhu R, Liu Z. Nitrogen-doped carbon cobalt grafted on graphitic carbon nitride catalysts with enhanced catalytic performance for ethylbenzene oxidation. J Mol Catal A: Chem 2016;420:11-7.

[16] Sturini M, Speltini A, Maraschi F, Vinci G, Profumo A, Pretali L, Albini A, Malavasi L. g-C_3N_4-promoted degradation of Ofloxacin antibiotic in natural waters under simulated sunlight. Environ Sci Pollut Res 2016;24;4153-61.

[17] Yang L, Huang J, Shi L, Cao L, Yu Q, Jie Y, Fei J, Ouyang H, Ye J. A surface modification resultant thermally oxidized porous g-C_3N_4 with enhanced photocatalytic hydrogen production. Appl Cat B: Environ 2017;204:335-45.

[18] Wang X, Maeda K, Thomas A, Takanabe K, Xin G, Carlsson JM, Domen K, Antonietti M. A metal-free polymeric photocatalyst for hydrogen production from water under visible light. Nat Mater 2009;8:76-80.

[19] Sun H, Zhou X, Zhang H, Tu W. An efficient exfoliation method to obtain graphitic carbon nitride nanosheets with superior visible-light photocatalytic activity. Int J Hydrogen Energy 2017;42:7930-7.

[20] Haleem YA, He Q, Liu D, Wang C, Xu W, Gan W, Zhou Y, Wu C, Ding Y, Song L. Facile synthesis of mesoporous detonation nanodiamond-modified layers of graphitic carbon nitride as photocatalysts for the hydrogen evolution reaction. RSC Adv 2017;7:15390-6.

411 [21] Yi SS, Yan JM, Wulan BR, Li SJ, Liu KH, Jiang Q. Noble-metal-free cobalt phosphide
412 modified carbon nitride: an efficient photocatalyst for hydrogen generation. Appl Cat B: Environ
413 2017; 200;477-83.
414
415 [22] Lin B, An H, Yan X, Zhang T, Wei J, Yang G. Fish-scale structured g-C_3N_4 nanosheet with
416 unusual spatial electron transfer property for high-efficiency photocatalytic hydrogen evolution.
417 Appl Cat B: Environ 2017;210:173-83.
418
419 [23] Lau VW, Yu VW, Ehrat F, Botari T, Moudrakovski I, Simon T, Duppel V, Medina E,
420 Stolarczyk JK, Feldmann J, Blum V, Lotsch BV. Urea-modified carbon nitrides: enhancing
421 photocatalytic hydrogen evolution by rational defect engineering. Adv Energy Mater
422 2017;7:1602251.
423
424 [24] L. Malavasi et al., manuscript in preparation.
425
426 [25] Fiol N, Villaescusa I. Determination of sorbent point zero charge: usefulness in sorption
427 studies. Environ Chem Lett 2009;7:79-84.
428
429 [26] Speltini A, Sturini M, Maraschi F, Dondi D, Fisogni G, Annovazzi E, Profumo A, Buttafava A.
430 Evaluation of UV-A and solar light photocatalytic hydrogen gas evolution from olive mill
431 wastewater. Int J Hydrogen Energy 2015;40:4303-10.
432
433 [27] Willett KL, Hites RA. Chemical actinometry: using *o*-nitrobenzaldehyde to measure light
434 intensity in photochemical experiments. J Chem Educ 2000;77:900-2.
435

436 [28] Speltini A, Sturini M, Dondi D, Annovazzi E, Maraschi F, Caratto V, Profumo A, Buttafava A.
437 Sunlight-promoted photocatalytic hydrogen gas evolution from water-suspended cellulose:
438 systematic study. Photochem Photobiol Sci 2014;13:1410-19.
439
440 [29] Xu Q, Cheng B, Yu J, Liu G. Making co-condensed amorphous carbon/g-C_3N_4 composites
441 with improved visible-light photocatalytic H_2-production performance using Pt as cocatalyst.
442 Carbon 2017;118:241-9.
443
444 [30] Ding N, Zhang L, Hashimoto M, Iwasaki K, Chikamori N, Nakata K, Xu Y, Shi J, Wu H, Luo
445 Y, Li D, Fujishima A, Meng Q. Enhanced photocatalytic activity of mesoporous carbon/C_3N_4
446 composite photocatalysts. J Colloid Interface Sci 2018;512:474-9.
447
448 [31] Fan C, Feng Q, Xu G, Lv J, Zhang Y, Liu J, Qin Y, Wu Y. Enhanced photocatalytic
449 performances of ultrafine g-C_3N_4 nanosheets obtained by gaseous stripping with wet nitrogen. Appl
450 Surf Sci 2018;427;730-8.
451
452 [32] Wen J, Xie J, Chen X, Li X. A review on g-C_3N_4-based photocatalysts. Appl Surf Sc. 2017;391
453 :72-123.
454
455 [33] Speltini A, Sturini M, Maraschi F, Dondi D, Serra A, Profumo A, Buttafava A, Albini A.
456 Swine sewage as sacrificial biomass for photocatalytic hydrogen gas production: explorative study.
457 Int J Hydrogen Energy 2014;39:11433-40.
458
459 [34] Fu X, Long J, Wang X, Leung DYC, Ding Z, Wu L, Zhang Z, Li Z, Fu X. Photocatalytic
460 reforming of biomass: a systematic study of hydrogen evolution from glucose solution. Int J
461 Hydrogen Energy 2008;33:6484-91.

[35] Li Y, Wang J, Peng S, Lu G, Li S. Photocatalytic hydrogen generation in the presence of glucose over ZnS-coated $ZnIn_2S_4$ under visible light irradiation. Int J Hydrogen Energy 2010;35:7116-26.

[36] Gu Q, Gao Z, Zhao H, Lou Z, Liao Y, Xu C. Temperature-controlled morphology evolution of graphitic carbon nitride nanostructures and their photocatalytic activities under visible light. RSC Adv 2015;5:49317-25.

[37] Badawy MI, Ghaly MY, Ali MEM. Photocatalytic hydrogen production over nanostructured mesoporous titania from olive mill wastewaters. Desalination 2011;267:250-5.

[38] Kisch H. On the problem of comparing rates or apparent quantum yields in heterogeneous photocatalysis. Angew Chem Int Ed 2010;49:9588-9.

[39] Daskalaki VM, Kondarides DI. Efficient production of hydrogen by photo-induced reforming of glycerol at ambient conditions. Catal Today 2009;144:75-80.

488 **Figure captions**

489 **Fig. 1** XRD patterns of as-prepared g-C_3N_4 (as-prep) and of oxidized g-C_3N_4 (3 h).

490

491 **Fig. 2** Representative SEM images of as-prepared (a) and oxidized g-C_3N_4 (b).

492

493 **Fig. 3** H_2 evolution rates as function of (a) glucose concentration (0.25 g L^{-1} catalyst, 3 wt% Pt,
494 native pH), (b) Pt loading (0.1 M glucose, 0.25 g L^{-1} catalyst, native pH); error bars represent the
495 standard deviation (RSDs < 6 %, *n*=3).

496

497 **Fig. 4** H_2 evolution rates as function of (a) catalyst concentration (0.1 M glucose, 3 wt% Pt, native
498 pH), (b) pH (0.1 M glucose, 3 wt% Pt, 0.25 g L^{-1} catalyst); error bars represent the standard
499 deviation (RSDs < 6 %, *n*=3).

500

501

502 **Table titles**

503 **Table 1.** H_2 evolution rates obtained from aqueous glucose using g-C_3N_4 or o-g-C_3N_4, and effect of
504 sonication; in parentheses is reported the standard deviation (RSD < 6 %, *n*=3).

505

506 **Table 2.** Comparison with 2017-2018 literature data about H_2 evolution from water using
507 differently modified g-C_3N_4 materials.

508

509 **Table 3.** H_2 evolution rates obtained under simulated or natural solar light, in different water
510 samples, using o-g-C_3N_4; in parentheses the standard deviation is reported (RSD < 5 %, *n*=3).

Table 1

	H_2 (μmoles g^{-1} h^{-1})[a]	
	No sonication	*Sonication (20 min)*
g-C_3N_4	16(1)	52(3)
o-g-C_3N_4	416(17)	870(35)

[a] Conditions: 1 M glucose, 0.25 g L^{-1} catalyst, 3 wt% Pt, solar simulated light.

Table 2

g-C_3N_4 precursor	H_2 production improvement factor[a]	Treatment	Photoproduction conditions	H_2 (μmoles g^{-1} h^{-1})	Ref.
Melamine	-	Thermal oxidation	Visible light (300 W Xenon lamp), 0.5 g L^{-1} catalyst, 3 wt% Pt, 10% TEOA	1501	[19]
Urea	1.5	Thermal condensation on nanodiamonds	Visible light, 1 g L^{-1} catalyst, 3 wt% Pt, 20% methanol	417	[20]
Melamine	4.3	Thermal oxidation (O_2 flow)	Visible light (300 W Xenon lamp, 562.89 mW cm^{-2}), 0.18 g L^{-1} catalyst, 3wt% Pt, 10% TEOA	1430	[17]
Urea	10	Thermal co-condensation urea + glucose	Visible light (350 W Xenon lamp), 0.62 g L^{-1} catalyst, 1 wt% Pt, 15% TEOA	213	[29]
Melamine	20	Thermal oxidation + solvothermal treatment	Visible light (300 W Xenon lamp), 1 g L^{-1} catalyst, 3 wt% Pt, 10% TEOA	1316	[22]
Urea	28	Functionalization by KSCN and HCl	Simulated solar light (300 W Xenon lamp), 1 g L^{-1} catalyst, 2wt% Pt, 10% methanol	2810	[23]
Melamine	1.5	Coupling with mesoporous carbon	Simulated solar light (300 W Xenon lamp), 0.5 g L^{-1} catalyst, 4wt% Pt, 10% TEOA	2040	[30]
Melamine	6	Gaseous stripping in wet N_2	Visible light (300 W Xenon lamp), 0.2 g L^{-1} catalyst, 3wt% Pt, 10% TEOA	1113	[31]
Dicyandiamide	26	Aqueous HNO_3 oxidation	Simulated solar light (Xenon lamp, 500 W m^{-2}), 1 g L^{-1} catalyst, 3	3280	This work

			wt% Pt, 10% TEOA		
Dicyandiamide	26	Aqueous HNO_3 oxidation	Simulated solar light (Xenon lamp, 500 W m^{-2}), 0.25 g L^{-1} catalyst, 3 wt% Pt, 1 M glucose	870	This work

[a] Modified/bulk g-C_3N_4 H_2 productions ratio

Table 3

	H_2 (μmoles g^{-1} h^{-1}) [a]	
	Simulated solar light[b]	*Natural sunlight*[c]
Distilled water	840(34)	-
River water	826(32)	-
Seawater	847(34)	2523(147)

[a] Conditions: 0.1 M glucose, 0.25 g L^{-1} o-g-C_3N_4 (sonication), 3 wt% Pt, native pH (*n*=3).
[b] 500 W m^{-2}.
[c] 797 W m^{-2} (global radiation average value).

Figure 1

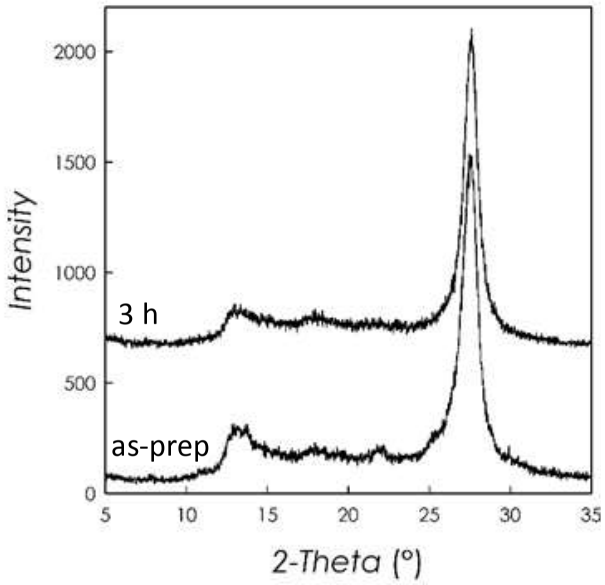
Intensity
2000
1500
1000
500
0
3 h
as-prep
5
10
15
20
25
30
35
2-Theta (°)

Figure 2

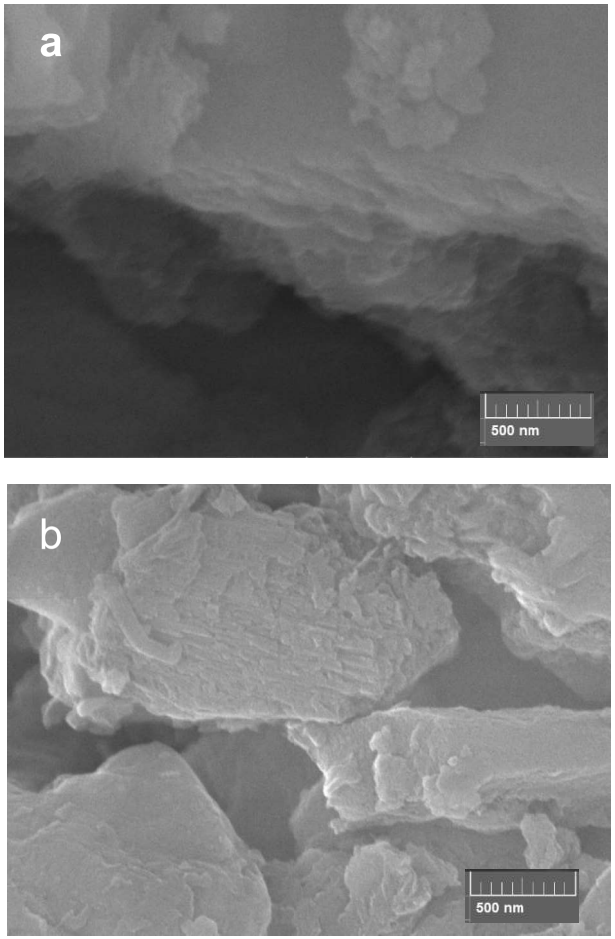

Figure 3

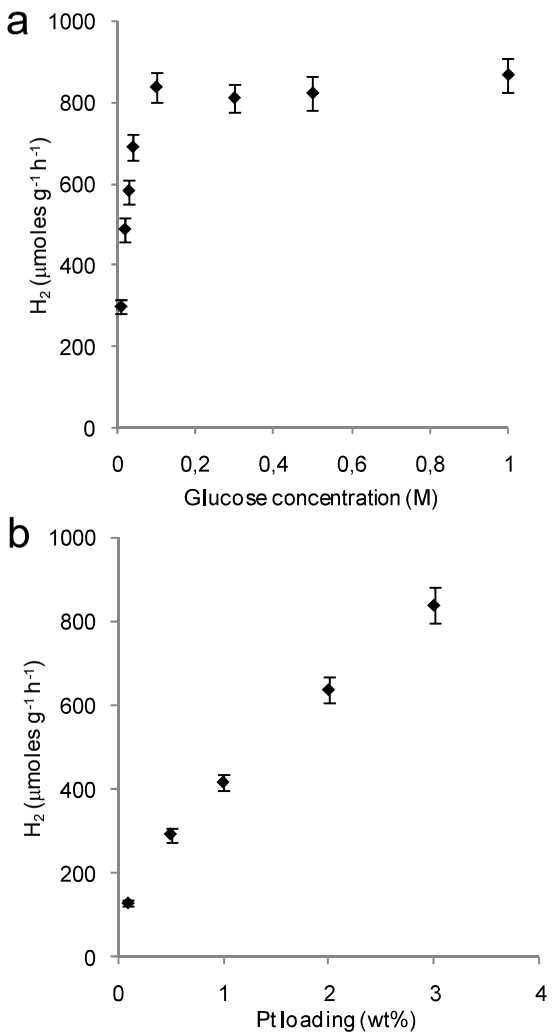
a
1000
800
600
400
200
0
H2 (µmoles g-1 h-1)
0
0,2
0,4
0,6
0,8
1
Glucose concentration (M)
b
1000
800
600
400
200
0
H2 (µmoles g-1 h-1)
0
1
2
3
4
Pt loading (wt%)

Figure 4

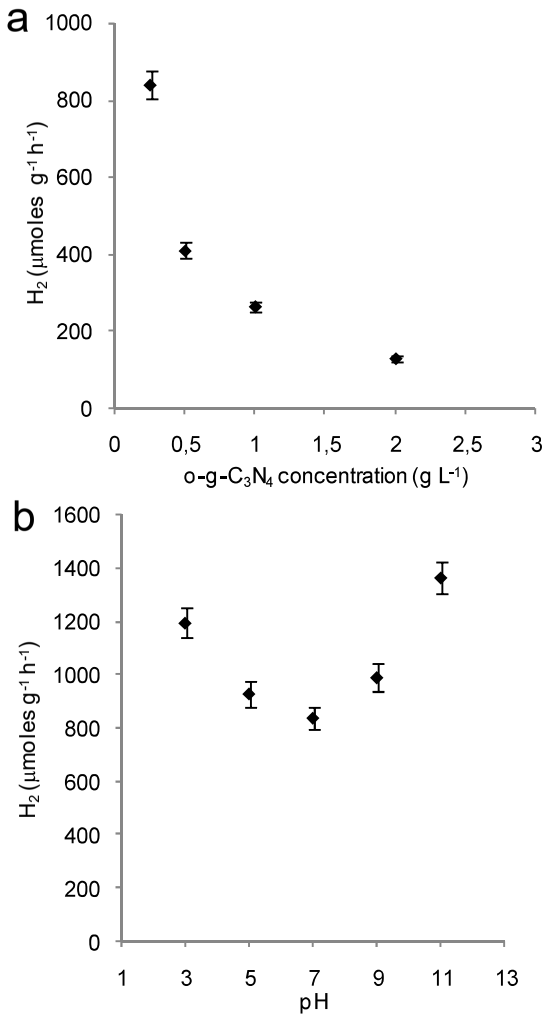
a
1000
800
600
400
200
0
H2 (µmoles g-1 h-1)
0
0,5
1
1,5
2
2,5
3
o-g-C3N4 concentration (g L-1)
b
1600
1400
1200
1000
800
600
400
200
0
H2 (µmoles g-1 h-1)
1
3
5
7
9
11
13
pH

Supplementary Material

Click here to download Supplementary Material: Supplementary Material.docx